JOURNAL OF MATERIALS SCIENCE 28 (1993) 2669–2676

Identification by DSC and DTA of the oxygen and carbon contamination due to the use of ethanol during mechanical alloying of Cu–Fe powders

F. FAUDOT, E. GAFFET, M. HARMELIN
CNRS, Centre d'Etudes de Chimie Métallurgique, 15, rue Georges Urbain, F-94407 Vitry-sur-Seine Cedex, France

Thermoanalytical methods (differential scanning calorimetry and differential thermal analysis) have been used in this work for characterizing Cu–Fe powder mixtures ball-milled with and without a liquid organic phase (ethanol). The effect of chemical contamination (carbon and oxygen) due to the use of ethanol is well evinced, as well as the benefit effect of ethanol on the surface properties of the powders (easier sintering). Strong and broad exothermic effects were observed during the decomposition of the metastable supersaturated solid solutions formed during ball-milling.

1. Introduction

One advantage of mechanical alloying, is the formation of metastable solid solutions with hitherto immiscible elements. Examples are Cu–Fe [1–4], Cu–Ta [5], Cu–V [6] and Cu–W [7]. On the other hand, the mechanical alloying of copper is a potential means of developing high-strength alloys maintaining high electrical and thermal conductivity [8].

In the Cu–Fe system, supersaturated b c c (Fe) solid solution up to about 30 at % Cu, and f c c (Cu) solid solution over about 60 at % Fe [1–4] were obtained by mechanical alloying, whereas equilibrium mutual solid solubility is less than 0.1 at % below 600 °C [9]. A quantitative thermodynamic explanation for the formation of solid solutions of immiscible elements by mechanical alloying has been proposed [10].

The use of a liquid organic phase (ethyl or methyl alcohol) during ball-milling in order to avoid excessive sticking of the powdered sample to the balls, was first reported in the Cu–Fe system [1, 2], but the resulting contamination was not investigated.

In this paper, the results of a detailed study by thermoanalytical techniques of the chemical contamination induced by the use of ethanol are reported. The two main techniques used, differential scanning calorimetry (DSC) and differential thermal analysis (DTA), allowed unambiguous characterization of the presence of Fe_3O_4 and Fe_3C formed by reaction between iron with oxygen and carbon resulting from the decomposition of ethanol during ball-milling. The complementarity of the thermal and structural investigations is shown. Moreover, ball-milling was performed under well-defined experimental conditions: the impact energy and frequency were strictly controlled during each experiment [4].

2. Experimental procedure

2.1. Ball-milling conditions

Starting materials were powders of copper (99.9%) and iron (> 99.5%). These powders were mixed to the desired composition. Two series of ball-milling were performed: (i) the initial Cu–Fe mixture (10 g) was sealed with the stainless steel balls in a cylindrical tempered stainless steel vial of capacity 45 ml, in an argon atmosphere and no ethanol was used: (ii) the same procedure was used but 1 cm^3 ethanol was added in the presence of air into the vial which was then sealed.

The mixtures were milled using a "G5"-type high-energy planetary ball mill which was designed and built at the CECM (CNRS, Vitry) [11, 12]. The rotation speed per minute (*r.p.m.*), Ω, of the disc on which the vial holders were fixed was 305 r.p.m. and the rotation speed, ω, of the vial holders was 675 r.p.m. The period of the milling was 240 h to obtain the steady state. Other experimental details are given elsewhere, [11, 12].

2.2. Scanning electron microscopy (SEM) and chemical energy dispersive microanalysis (EDX)

The particle morphology was characterized using a digital scanning electron microscope (Zeiss DSM 950) in the secondary electron image mode [4]. In order to evaluate the change in the composition after ball-milling and the possible contamination which may have occurred by friction of the powdered particles on the balls and on the walls of the vials, EDX analysis on large surfaces (in scanning mode) was performed using

0022–2461

a Si–Li detector and a Tracor EDX analyser in conjunction with the scanning electron microscope.

2.3. X-ray diffraction (XRD)

After ball-milling, a sample of powder was extracted from the vial and glued onto a silica plate for X-ray investigations. The X-ray diffraction patterns were obtained using a $(\theta - 2\theta)$ Philips diffractometer with CoK_α radiation. Two numerical methods (the so-called "ABFfit" and the "APD" programs) were used in order to determine the particle size of the powder and the lattice parameter of the various phases. They are described in details elsewhere [13].

2.4. Differential thermal analysis (DTA) and differential scanning calorimetry (DSC)

The advantage of DSC over DTA is the great flexibility and accuracy of the heat treatments applied to the samples. The disadvantage is the low upper-limit temperature (725 °C) of the heat treatments.

DTA measurements were carried out using the Setaram M4-microDTA device. 80 mg powder were put into alumina crucibles and heated and cooled at a rate of 10 °C min^{-1} between room temperature and 850 °C. During all measurements, a 100 ml min^{-1} argon flow was maintained. The DSC experiments were performed with a Perkin–Elmer DSC-2C apparatus equipped with a 3600 thermal analysis data station. About 50 mg samples were enclosed in copper pans and heated at 40 °C min^{-1} in argon up to 725 °C. The cooling rate was 320 °C min^{-1}. Several successive thermal cycles were carried out in order to study the reversibility of the thermal events.

3. Results

3.1. EDX analysis

Iron and Chromium contents were quantitatively determined after ball-milling. The results are listed in Table I. The advantage of using a liquid organic phase (here ethanol) during ball-milling is clearly seen: when ethanol is used, the final composition of the ball-milled powder is closer to the composition of the initial mixture and the chromium contamination is decreased. Hereafter, for clarity, the composition of the samples will be referred to by two values: that of the initial composition followed in parentheses by the measured composition of the end product.

TABLE I EDX analysis results: iron content of the powders before (i) and after (f) ball-milling and chromium content after ball milling. Note that the differences between the final iron content and the initial iron content and chromium contamination are less when ethanol is used during ball-milling [4] (all values in wt %). n.p., not prepared

Without ethanol			With ethanol	
Fe (i)	Fe (f)	Cr	Fe (f)	Cr
0	12.7	≤ 0.8	n.p.	n.p.
10	22.1 ± 0.9	≤ 1.0	9.6 ± 0.3	≤ 0.1
20	31.9 ± 0.8	≤ 0.5	22.6 ± 0.4	≤ 0.2
30	40.0 ± 4.0	≤ 1.2	31.9 ± 0.4	≤ 0.1
40	60.7 ± 1.2	≤ 2.5	42.9 ± 0.4	≤ 0.1
50	62.1 ± 4.6	≤ 1.5	54.7 ± 0.9	≤ 0.2
60	64.5 ± 0.3	≤ 1.8	65.3 ± 0.4	≤ 0.3
65	66.8 ± 0.3	≤ 1.3	n.p.	n.p.
70	73.0 ± 1.8	≤ 0.7	78.2 ± 0.5	≤ 1.0
80	82.4 ± 0.3	≤ 0.4	94.0 ± 0.9	≤ 0.2
90	90.5 ± 0.4	≤ 0.4	n.p.	n.p.
100	≈ 100	≤ 0.5	n.p.	n.p.

TABLE II Structure and composition range of the various phases formed after ball-milling with and without ethanol

Phases	Without ethanol	With ethanol
bcc(Fe)	0–27 wt % Cu	0–20 wt % Cu
fcc(Cu) + bcc(Fe)	65–67 wt % Fe	65–78 wt % Fe
fcc(Cu)	0–62 wt % Fe	0–65 wt % Fe

3.2. XRD

The results are summarized in Table II.

An example of the XRD patterns obtained for Fe = 20 (22), 60 (65) and 80 (94) wt % Fe ball-milled with ethanol is shown in Fig. 1. For Cu–20 (22) wt % Fe, the fcc (Cu) peaks are fine and all visible, whereas for Cu–80 (94) wt % Fe, broad bcc (Fe) peaks only are present. For the intermediate composition, Cu–60 (65) wt % Fe, both bcc (Fe) and fcc (Cu) peaks are observed. This result is in agreement with the formation of supersaturated crystalline (iron) and (copper) solid solutions during ball-milling.

Additional peaks with very weak intensity are also detected in Fig.1. For Cu–20 (22) wt % Fe, they have been identified as corresponding to the presence of small amounts of Fe_3O_4, and for Cu–80 (94) wt % Fe by the presence of Fe_3C. This interpretation has been clearly checked by the DTA and DSC investigations described below.

The values of the respective lattice parameters a (Fe) and a (Cu) determined for all compositions with and without ethanol are reported elsewhere [4].

When ball-milling is carried out with ethanol, the supersaturated bcc (Fe) solid solution extends from 0 to ≈ 20 wt % Cu, whereas the supersaturated fcc (Cu) solid solution extends in the range from 0 to ≈ 65 wt % Fe with a linear relationship of the lattice parameter versus the iron content, C_{Fe}. In this range of composition, the Vegard law has been calculated as

$$a(\text{Cu}) = 0.3619 + 4.3448 \times 10^{-5} C_{Fe} \quad (1)$$

where a (Cu) is expressed in nanometres and C_{Fe} is the iron content (wt %) of the ball-milled product.

When ball-milling is carried out without ethanol, no extra peaks corresponding to Fe_3O_4 and Fe_3C are detected and the supersaturated bcc (Fe) solid solution is more extended, from 0 to ≈ 27 wt % Cu. In this range of composition, the change in the lattice parameter versus the copper content, C_{Cu}, is linear. The Vegard law has been calculated as

$$a(\text{Fe}) = 0.2877 + 1.626 \times 10^{-5} C_{Cu} \quad (2)$$

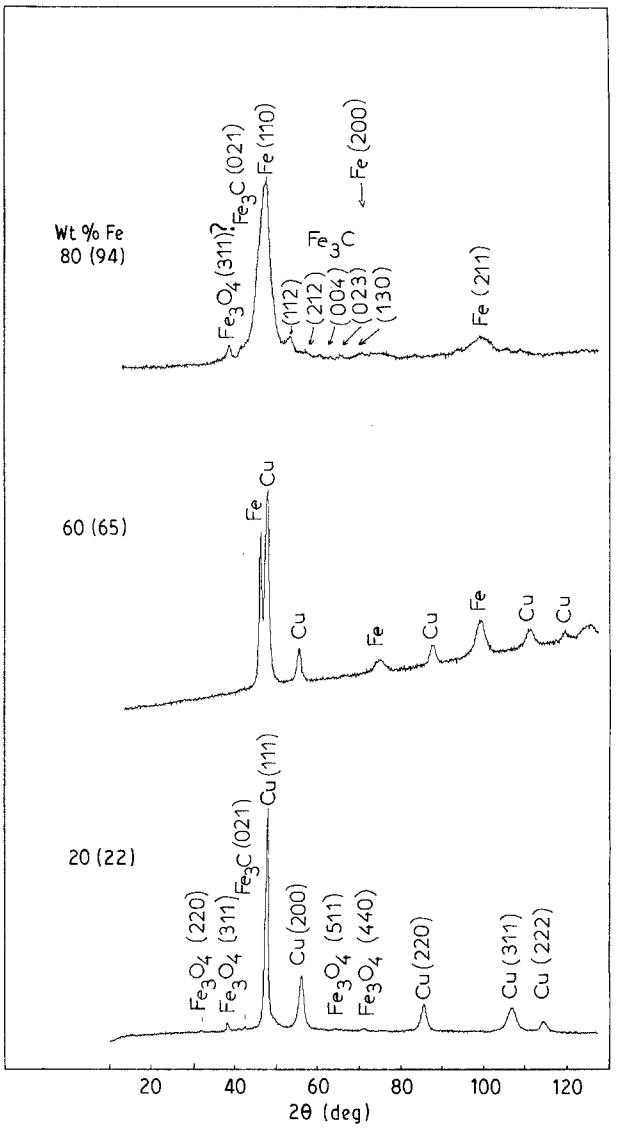

Figure 1 X-ray diffraction patterns for Cu–Fe samples ball-milled with ethanol (Fe = 20 (22), 60 (65) and 80 (94) wt %). For the samples ball-milled without ethanol the lines due to Fe_3O_4 and Fe_3C are not observed.

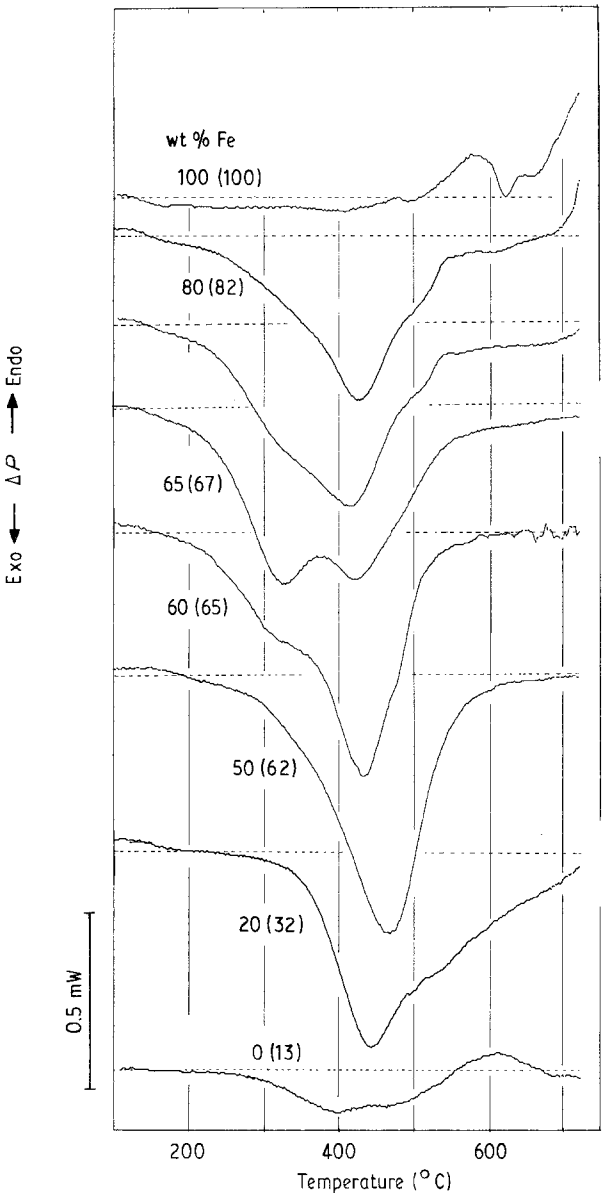

Figure 2 DSC curves obtained with samples ball-milled without ethanol. All curves are normalized to 1 mg sample weight.

where a (Fe) is expressed in nanometres and C_{Fe} is the iron content (wt %) of the ball-milled product. The supersaturated fcc (Cu) solid solution extends in the range of $\approx$0–62 wt % Fe, but no relationship between the lattice parameter and the iron content may be found. Indeed, the supersaturated fcc (Cu) solid solution is not well homogenized in terms of iron content, so the X-ray study only accounts for an average measure of the parameter (for more details, see Gaffet *et al.* [4]).

In the intermediate range, both bcc (Fe) and fcc (Cu) phases coexist.

It is worth noting that for all compositions the presence of a slight volume fraction of an amorphous phase has been detected on applying the ABFfit and APD programs to the XRD patterns [4, 14].

3.3. DSC and DTA

The DSC curves obtained with powders ball-milled without ethanol are shown in Fig. 2. The major feature is an exothermic peak from 200 to $\sim$ 600 °C slightly split for some compositions. This exothermic effect is no longer observed on heating the same specimen a second time: it is therefore irreversible.

The DSC curves obtained with the powders ball-milled with ethanol are shown in Fig. 3. They are much more complicated. Exothermic effects are also detected from 200 to $\sim$600 °C but they are superimposed with endothermic peaks at 300–400 °C and 580–600 °C, respectively. The highest intensity of the endothermic peak is observed for the lowest iron content (10 wt %). This endothermic effect is irreversible as shown in Fig. 4a and b. During the second heating (Fig. 4b) an exothermic peak between 250 and 350 °C and an endothermic peak at 581 °C are detected. These effects will be explained below. For iron compositions ranging from 50–80 wt % (Fig. 3), the DSC curves show the beginning of another endothermic effect above 700 °C. The complete investigation of this effect for all compositions has been carried out by DTA on heating up to 850 °C and cooling to room

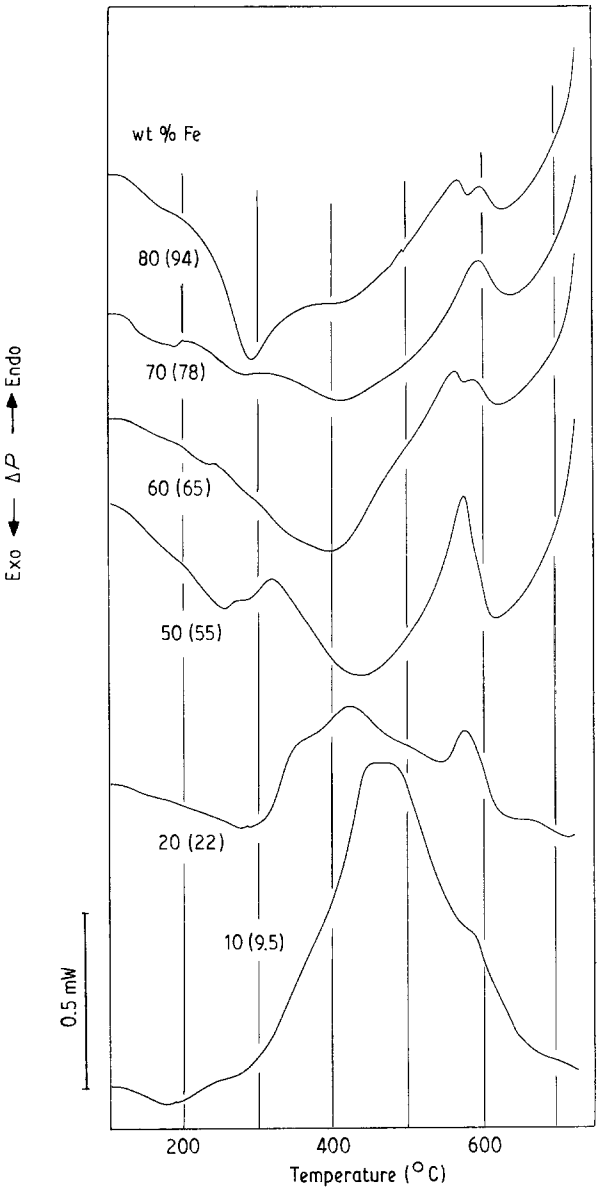

Figure 3 DSC curves obtained with samples ball-milled with ethanol. All curves are normalized to 1 mg sample weight.

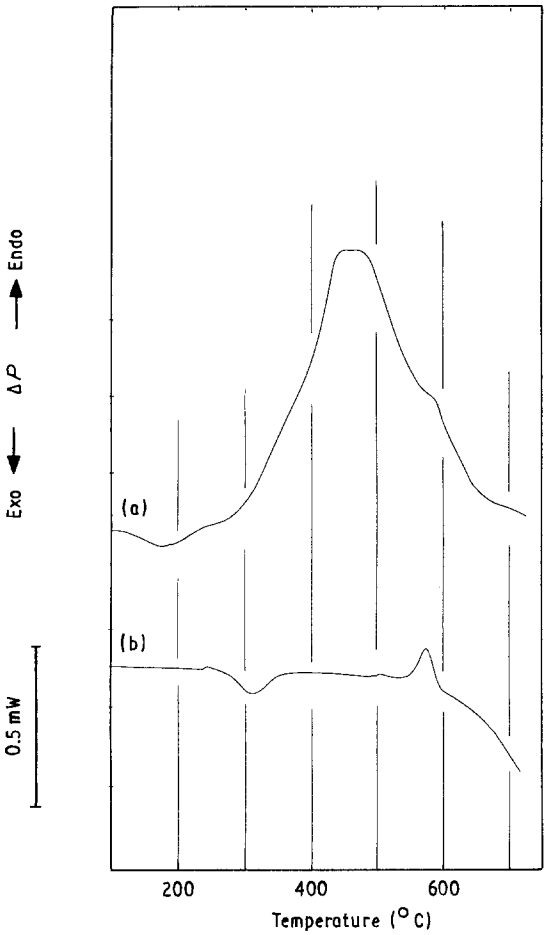

Figure 4 DSC curves for Cu–10 wt % Fe ball-milled with ethanol. (a) First heating: evidence of an intense endothermic effect due to the shrinkage of the sample on sintering. (b) Second heating of the same specimen. The endothermic effect is no longer observed and additional exothermic and endothermic peaks due to the reversible reaction (α-Fe) + $Fe_3O_4 \rightleftharpoons$ FeO [16] are now detected.

temperature. The respective curves are shown in Fig. 5a and b. The endothermic effect at 720 °C on heating corresponds to an exothermic effect at $\approx$690 °C on cooling; the reaction involved is thus reversible. The amplitude of the endothermic and exothermic effects increases when the iron content is increased.

4. Discussion

In order to interprete the results described above, a series of heat cycles with the same samples has been performed in the DSC between 50 and 725 °C for all compositions. An example is shown for Cu–80 (94) wt % Fe (Fig. 6). The complete results with their interpretation are given for all compositions in Table III. For all experiments, the cooling rate was 320 °C min^{-1}.

4.1. The exothermic effects between 200 and 600 °C

These irreversible effects are due to the decomposition of the supersaturated bcc (Fe) and fcc (Cu) solid solutions into the equilibrium phases, i.e. almost pure bcc Fe and fcc Cu phases. Some exothermic contribution of the crystallization of the amorphous phase can also be expected but it is probably very weak because the volume fraction of the amorphous phase is small. It cannot, therefore, be distinguished from the major effect due to the decomposition of the metastable solid solutions.

4.2. The endothermic effect at 300–400 °C

This effect, observed only with the samples ball-milled with ethanol, is interpreted by the sintering of the particles on heating. This effect is, of course, irreversible on cooling. Although sintering is basically an exothermic process [15], it is detected as an endothermic one when differential calorimetric techniques are applied. This is due to the spurious effect of the shrinkage on sintering. The progressive shrinkage of the powdered sample which occurs on sintering modifies the thermal contact with the crucible and results in a drastic decrease of the heat transfer coefficient between the sample and the thermal sensor. Because this effect does not occur on the reference side, a negative temperature difference between

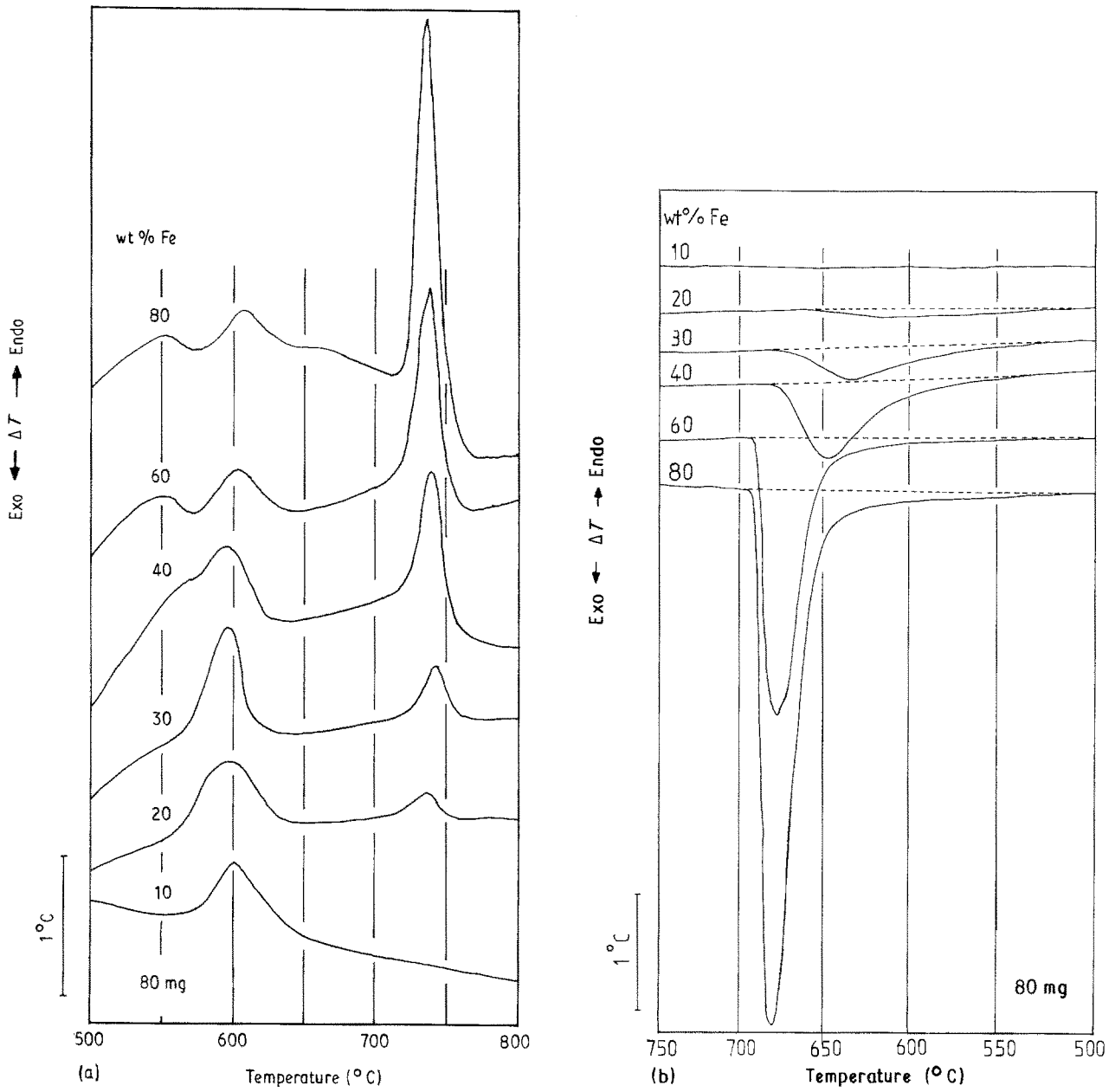

Figure 5 DTA curves on (a) heating and (b) cooling samples at 10 °C min^{-1} of various compositions ball-milled with ethanol. The endothermic and exothermic effects give evidence of the reversible reaction (α-Fe) + $Fe_3C \rightleftharpoons$ (γ-Fe) at 723 °C [16].

sample and reference is detected by the heat sensor and is responsible for the endothermic effect.

The sintering of the powders was only detected by DSC when ball-milling was performed with ethanol. It increased when the copper content was increased. This was probably due to the specific superficial properties of the powders and to the influence of copper for the easy formation of necking between elemental particles.

4.3. The endothermic effects at 560 and 600 °C

When the samples were ball-milled with ethanol, the presence of Fe_3O_4 was detected on the X-ray diffraction patterns especially for low iron contents [4]. By referring to the phase diagrams Fe–O [16], it can be expected that when the phase Fe_3O_4 is heated in the presence of α-Fe, the following eutectoid reaction would proceed at 570 °C

$$(\alpha\text{-Fe}) + Fe_3O_4 \rightarrow FeO \quad (3)$$

This reaction is reversible on cooling.

The eutectoid Reaction 3 at 570 °C therefore allows the magnetite Fe_3O_4 to be characterized by DSC and DTA by an endothermic effect on heating. In the present case, the temperature determined by DTA and DSC for this invariant reaction was slightly higher (≈600 °C, see Table III), probably for kinetic reasons. Reaction 3 is a solid-state reaction which needs time to proceed and its achievement is thus heating-rate dependent. The series of heat cycles described in Fig. 6 allows one to understand the kinetic factors related to Reaction 3. Because the cooling rate from 725 °C to room temperature was high (320 °C min^{-1}), the reverse Reaction 3 is avoided on cooling and can only

TABLE III Curie temperature of Fe_3C and Fe_3O_4, and peak temperature of the reaction (α-Fe) + $Fe_3O_4 \rightleftharpoons FeO$, determined by DSC for several successive heating cycles of the same sample of Cu–Fe powders ball-milled with ethanol. The reaction $FeO \rightarrow$ (α-Fe) + Fe_3O_4 was not observed during the rapid cooling from 725 °C, but was on reheating. For ΔQ, the negative sign indicates an exothermic effect and the positive sign an endothermic one. n.d. not detected; e, end of the heat cycle; T_{max}, the upper limit temperature of each heating cycle

Fe	Heat	Fe_3C	Fe_3O_4	(α-Fe) + $Fe_3O_4 \rightarrow FeO$		T_{max}	$FeO \rightarrow$ (α-Fe) + Fe_3O_4	
(wt %)	cycle	(°C)	(°C)	(°C)	ΔQ (J g^{-1})	(°C)	(°C)	ΔQ (J g^{-1})
10 (9.5)	1	?	n.d.	585	n.d.	725	315	− 6
	2	n.d.	510?	581	+ 5	725	n.d.	n.d.
20 (22)	1	≈205?	n.d.	580	+ 9	725	335	− 13
	2	203.0	560	599	+ 11	725	340	− 12
	3	202.9	–	–	–	450	330	− 2
	4	203.8	–	–	–	450	–	0
	5	205.7	–	–	–	450	–	0
	6	207	561	602	+ 13	725	344	− 12
	7	204.8	561	602	+ 10	725	n.d.	n.d.
30 (32)	1	≈205?	n.d.	583	+ 11	725	317	− 14
	2	205.8	n.d.	592	+ 10	725	323	− 14
	3	204.1	–	–	–	450	319	− 2.0
	4	204.3	n.d.	593	+ 12	725		
40 (43)	1	≈205?	577	596	n.d.	725	325	− 15
	2	205.7	565	597	+ 10	725	334	− 13
	3	205.2	–	–	–	450	328	− 2
	4	204.8	–	–	–	450	–	0
	5	204.7	562	599	+ 11	725	339	− 13
	6	205.4	562	601	+ 10	725	e	e
50 (55)	1	≈205?	576	597	n.d.	725	333	− 17
	2	204.8	565	602	+ 12	725	344	− 17
	3	204.6	–	–	–	450	e	e
60 (65)	1	≈205?	567	591	n.d.	725	331	− 11
	2	206.7	560	610	+ 8	725	340	− 10
	3	205.2	–	–	–	450	–	0
	4	206.7	560	612	+ 7	725	346	− 11
	5	205.7	560	613	+ 8	725	e	e
70 (78)	1	≈205?	n.d.	595	n.d.	725	357	− 8
	2	208.0	524	627	+ 5	725	362	− 7
	3	206.9	–	–	–	450	361	− 1
	4	207.0	–	–	–	450	–	0
	5	207.5	?	628	+ 6	725	369	− 7
	6	207.4	550?	628	+ 7	725	e	e
80 (94)	1	≈205?	569	599	n.d.	725	329	− 10
	2	206.8	560	614	+ 7	725	335	− 10
	3	205.5		–	–	725	–	0
	4	205.4		–	–	450	–	0
	5	206.7	544?	617	+ 8	450	342	− 9
	6	206.1	555	618	+ 8	725	e	e

proceed on further heating at a lower rate. The intensity and the temperature range of the peak, measured for different cooling rates, are reported in Table IV. The lower the cooling rate, the higher is the peak intensity. For 320 °C min^{-1}, FeO is maintained as a metastable phase to room temperature and the exothermic reaction $FeO \rightarrow (Fe_\alpha) + Fe_3O_4$ proceeds when the temperature is high enough (> 250 °C) to enable diffusion for establishing the equilibrium state.

The intensity, ΔQ, of the exothermic and endothermic effects resulting from the eutectoid reaction (α-Fe) + $Fe_3O_4 \rightleftharpoons FeO$ is reported in Table III. This intensity is proportional to the amount of Fe_3O_4 in the powder. It remains generally of the same order of magnitude on heating and cooling and is not highly dependent on the composition in contradiction to the XRD results which detected the upper limit of Fe_3O_4 at 32 wt % Fe [4]. Because the enthalpy, ΔH, of the reaction is unknown to our knowledge, the corresponding amounts of Fe_3O_4 could not be calculated. It can thus be concluded from the DSC measurements that (i) the contamination from oxygen is of the same order of magnitude for all compositions and (ii) DSC is more sensitive than XRD for detecting the traces of Fe_3O_4.

Because the Curie temperature of Fe_3O_4 is reported in the literature to be at 575 °C [16], Fe_3O_4 can also be expected to be detected as an endothermic effect on heating in this temperature range. An example is given in Fig. 6 for 80 (94) wt % Fe. It is worth noting that for this composition Fe_3O_4 is hardly detected. The phenomenon has been characterized at slightly lower temperatures (see Table III), probably because of a lack of purity of the phase.

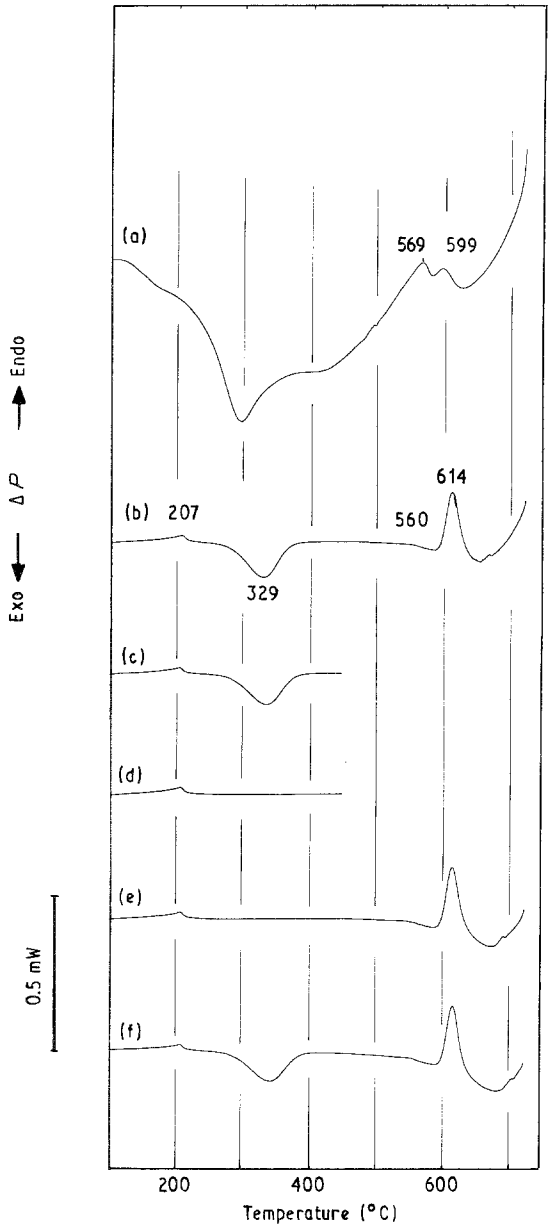

Figure 6 DSC analysis of the reversibility of the various reactions for Cu–80 wt % Fe ball-milled with ethanol. The same sample was successively heated to (a, b) 725 °C, (c, d) 450 °C and (e, f) again at 725 °C. Cooling rate was 320 °C min^{-1}.

4.4. The endothermic effects at 205 and 720 °C

When the samples were ball milled with ethanol, the presence of Fe_3C was also detected on the X-ray diffraction patterns, especially for high iron contents [4]. By referring to the phase diagram Fe–C [16], it can be expected that when the phase Fe_3C is heated in the presence of α-Fe, the following eutectoid reaction would proceed at 723 °C,

$$(\alpha\text{-Fe}) + Fe_3C \rightarrow (\gamma\text{-Fe}) \quad (4)$$

This reaction is reversible on cooling.

This was clearly confirmed by DTA (see Fig. 5). Cementite, Fe_3C, is revealed at about 720 °C by an endothermic effect corresponding to Reaction 4. It can be seen in Fig. 5 that the intensity of the endothermic (or exothermic) reactions increases with the iron content. This result explains why Fe_3C is hardly detected by X-ray diffraction below 40 wt % Fe [4].

Fe_3C was also characterized by DSC by its Curie temperature reported at 210 °C [16]. The Curie temperature of Fe_3C is badly detected by DSC on the first heating for all compositions (Figs 3, 4 and 6) but is well visible after the first heating to 725 °C. This behaviour is probably due the presence of structural defects in the ball-milled powders.

TABLE IV Intensity, ΔQ, and temperature range of the reaction $FeO \rightarrow (Fe_\alpha) + Fe_3O_4$ determined by DSC, for different cooling rates after the first heating, for a Cu–80 (94) wt % Fe alloy. For ΔQ, the negative sign indicates an exothermic effect

Cooling rate (°C min^{-1})	$FeO \rightarrow (Fe_\alpha) + Fe_3O_4$	
	Peak intensity, ΔQ (J g^{-1})	Temperature range (°C)
320	0	–
40	− 3	450–230
10	− 5	420–250

5. Conclusion

The following useful information has been found by the thermoanalytical techniques (DSC and DTA) used in this work for investigating Cu–Fe ball-milled powders.

1. In the chemical contamination due to the use of ethanol during ball milling, the presence of Fe_3O_4 and Fe_3C formed by reaction of iron with oxygen and carbon resulting from the decomposition of ethanol during ball milling is evinced by endothermic effects on heating, corresponding to the eutectoid reactions $(\alpha\text{-Fe}) + Fe_3O_4 \rightarrow FeO$ at ≈ 600 °C and $(\alpha\text{-Fe}) + Fe_3C \rightarrow (\gamma\text{-Fe})$ at ≈ 720 °C, respectively.

2. Investigation of the structural state of the powders has shown that extended metastable supersaturated fcc (Cu) and bcc (Fe) solid solutions were obtained by mechanical alloying. On further heating, intense exothermic effects were observed by DTA or DSC and revealed the decomposition of the solid solutions into equilibrium almost pure copper and iron.

3. The surface state of the powders was investigated; sintering of the powders occurred on heating only when ball-milling was performed with ethanol. This phenomenon is revealed by an endothermic effect on the DSC curves.

References

1. P. H. SHINGU, K. N. ISHIHARA, K. UENISHI, J. KUYAMA, B. HUANG and S. NASU, in "Solid State Powder Processing", edited by A. H. Clauer and J. J. de Barbadillo (The Minerals, Metals and Materials Society, 1990) p. 21.
2. K. UENISHI, K. F. KOBAYASHI, S. NASU, H. HATANO, K. N. ISHIHARA and P. H. SHINGU, *Z. Metallkde* **83** (1992) 132.

3. A. R. YAVARI, P. J. DESRE and T. BENAMEUR, *Phys. Rev. Lett.* **68** (1992) 2235.
4. E. GAFFET, M. HARMELIN and F. FAUDOT, *J. Alloys Compounds*, in press.
5. G. VELTL, B. SCHOLZ and H. D. KUNZE, *Mater. Sci. Engng* **A134** (1991) 1410.
6. T. FUKUNAGA, M. MORI, K. INOUE and U. MITZUTANI, *ibid.* **A134** (1991) 863.
7. E. GAFFET, C. LOUISON, M. HARMELIN and F. FAUDOT, *ibid.* **A134** (1991) 1380.
8. D. G. MORRIS and M. A. MORRIS, *Scripta Metall. Mater.* **24** (1990) 1701.
9. W. G. MOFFATT, "Handbook of binary phase diagrams", Vol. 2 (Genium, New York, 1984).
10. A. R. YAVARI and P. J. DESRE, in "Ordering and disordering in Alloys", edited by A. R. Yavari (Elsevier Applied Science, London, 1992) p. 414.
11. E. GAFFET, *Mater. Sci. Engng* **A132** (1991) 181.
12. E. GAFFET and L. YOUSFI, *Mater. Sci. Forum* **88-90** (1992) 51.
13. E. GAFFET and M. HARMELIN, *J. Less-Common Metals* **157** (1990).
14. E. GAFFET, F. FAUDOT and M. HARMELIN, *Mater. Sci. Forum* **88-90** (1992) 375.
15. Y. H. ZHOU, M. HARMELIN, J. BIGOT, *Scripta Metall.* **23** (1989) 1391 and *Mém. Sci. Rev. Métall.* (1990) 93.
16. A. MICHEL, in "Nouveau traité de Chimie Minérale", 1st Edn, edited by P. Pascal XVII (Masson, Paris, 1967) pp. 600 831.

Received 3 September
and accepted 30 October 1992